

Journal of Materials Chemistry A

Accepted Manuscript



This is an *Accepted Manuscript*, which has been through the Royal Society of Chemistry peer review process and has been accepted for publication.

Accepted Manuscripts are published online shortly after acceptance, before technical editing, formatting and proof reading. Using this free service, authors can make their results available to the community, in citable form, before we publish the edited article. We will replace this *Accepted Manuscript* with the edited and formatted *Advance Article* as soon as it is available.

You can find more information about *Accepted Manuscripts* in the [Information for Authors](#).

Please note that technical editing may introduce minor changes to the text and/or graphics, which may alter content. The journal's standard [Terms & Conditions](#) and the [Ethical guidelines](#) still apply. In no event shall the Royal Society of Chemistry be held responsible for any errors or omissions in this *Accepted Manuscript* or any consequences arising from the use of any information it contains.

Cite this: DOI: 10.1039/c0xx00000x

www.rsc.org/xxxxxx

Full Article

Efficient Inverted Quasi-Bilayer Organic Solar Cells Fabricated by Using Non-Halogenated Solvent Processes

Jung-Hao Chang,^a Hsiao-Fang Wang,^b Wei-Chieh Lin,^a Kai-Ming Chiang,^a Kuan-Chen Chen,^a Wei-Ching Huang,^a Zheng-Yu Huang,^a Hsin-Fei Meng,^c Rong-Ming Ho^b and Hao-Wu Lin^{*a}

Received (in XXX, XXX) XthXXXXXXXXXX 20XX, Accepted Xth XXXXXXXXXXXX 20XX

DOI: 10.1039/b000000x

Here we demonstrate the fabrication of novel, “quasi-bilayer” inverted organic photovoltaic devices using halogen-free solvents. The inferior solubility of pristine fullerene in non-halogenated solvents was used to control the interpenetration of upper polymeric donor layers with bottom fullerene layers. Notably, island-like nano-morphologies were revealed by AFM, SEM, TEM, cross-sectional TEM images and PL quenching measurement. Correlation between device performance, thin-film nano-morphology and ac impedance was observed. High efficiencies of 6.55% and 7.15% were observed for PBDTTT-C-T and PTB7 cells, respectively. These results demonstrate that this novel process not only offers an effective new method to control the morphology of solar active layers but, more importantly, could also be applied to a wide range of current material systems to produce efficient devices that comply with the non-toxic halogen-free requirement.

1. Introduction

Organic solar cells (OSCs) have gained tremendous attention because of their unique properties, such as low-cost fabrication, low-energy consumption, roll-to-roll processing, semi-transparency and mechanical flexibility, which are required for variety of applications.¹⁻⁸ OSCs fabricated with two fundamental architectures, bilayer configuration or bulk-heterojunction (BHJ), have demonstrated promising power conversion efficiencies (PCEs) of approximately 7-10%.⁹⁻¹⁶ In bilayer devices, the solar active layers are formed by sequential layer-by-layer deposition of donor and acceptor materials,¹⁷⁻²¹ whereas in BHJ devices, the active layer is formed by a single film composed of a mixture of donor and acceptor materials.²²⁻²⁴ It was recently reported that solution-processed OSCs with a bilayer structure produced an interfacial BHJ layer between the neat donor and acceptor films, which provided a new method to control the degree of intermixing between the donor and acceptor.²⁵⁻³¹ In the aforementioned “quasi-bilayer” devices, [6,6]-phenyl-C₆₁-butyric acid methyl ester (PC₆₁BM) or [6,6]-phenyl-C₇₁-butyric acid methyl ester (PC₇₁BM) was used as the electron accepting material. Because PCBM is highly soluble in common solvents, the device usually utilizes a bottom polymer layer with relatively poor solubility onto which an upper PCBM layer is sequentially solution-cast. A certain degree of interpenetration of the PCBM into the polymer layer occurs, and a mixed donor-acceptor quasi-bilayer structure is formed.^{28, 29}

In these “quasi-bilayer” studies, and in most BHJ devices, halogenated aromatic solvents (e.g., chlorobenzene, dichlorobenzene, dichloromethane or chloroform) were selected for device preparation.³²⁻³⁶ Although the solubilities of polymers and fullerenes in halogenated aromatic solvents are typically significantly higher than those in halogen-free solvents, which makes device fabrication much easier, halogenated solvents are more toxic. This limits their potential mass use in

environmentally friendly production. Therefore, the use of halogen-free solvents for the preparation of OSCs has been increasingly investigated.³⁷⁻³⁹ In this regard, Alex K.-Y. Jen et al. have demonstrated the fabrication of an efficient BHJ solar cell with an impressively high PCE of up to 6 ~ 7% by utilizing non-halogenated solvent mixture with 1-methylnaphthalene as additive.^{40, 41}

In this work, we report the fabrication of a highly efficient inverted quasi-bilayer OSC using non-halogenated solvent processes. The interpenetration of the upper donor layer and the bottom fullerene layer was well controlled by taking advantage of the reduced solubility of pristine fullerene in non-halogenated solvents (solubility of C₇₀ in toluene and *o*-xylene is ~1.4 mg/ml and ~3.9 mg/ml, respectively). By using the rapid-drying blade-coating technique,^{42, 43} “quasi-bilayer” structures were obtained *in situ* within a short period of time (less than one second) without any post-thermal or solvent annealing. Interpenetration was confirmed by atomic force microscopy (AFM), scanning electron microscopy (SEM), transmission electron microscopy (TEM) and cross-sectional TEM images.⁴⁴ Utilizing these quasi-layers, conceptual devices were fabricated and characterized based on the following small-bandgap polymers: poly[4,8-bis-(2-ethylhexyl-thiophene-5-yl)-benzo[1,2-*b*:4,5-*b'*]dithiophene-2,6-diyl]-alt-[2-(2'-ethyl-hexanoyl)-thieno[3,4-*b*]thiophen-4,6-diyl](PBDTTT-C-T)⁴⁵⁻⁴⁷ and thieno[3,4-*b*]thiophene/benzodithiophene(PTB7)⁴⁸⁻⁵². Under simulated 1-sun AM 1.5G illumination, high PCEs of 6.55% and 7.15% were observed for the PBDTTT-C-T and PTB7 cells, respectively. These results reveal that the process not only offers an effective way to control the morphology of active solar layers but also could be applied to a wide range of material systems for the production of efficient devices that comply with the non-toxic

halogen-free requirement.

2. Experimental

2.1 Device fabrication

PBDTTT-C-T and PTBT were purchased and used as received from Solarmer Energy, Inc. and I-Materials, respectively. Before use, the C₇₀ was subject to purification by temperature-gradient sublimation in a high vacuum chamber (pressure $\sim 1 \times 10^{-6}$ Torr). Devices were fabricated with the structure of ITO/Ca/C₇₀/PBDTTT-C-T or PTB7/MoO₃/Ag. ITO glass (sheet resistance: $\sim 15 \Omega/\text{sq}$) was cleaned in an ultrasonic bath with de-ionized water, acetone, and methanol for 15 min, successively. A hole blocking cathode, Ca, and acceptor layer, C₇₀, were deposited onto the ITO glass in a high vacuum chamber with a base pressure of $\sim 1 \times 10^{-6}$ Torr. The polymers were dissolved in toluene (9 mg/ml) and *o*-xylene (9 mg/ml). The co-solvent process was performed by mixing the *o*-xylene solution into the toluene solution at varying proportions ranging from 0 to 20 wt%. The polymer solution was then cast onto the bottom C₇₀ layer by fast-drying blade-coating method with blade speed ranging from 60 to 350 mm/s (controlled by a servomotor). The blade-coating process was performed on a hot plate at 90 degrees Celsius, and the polymer film dried in < 1 sec (see Table S1). The films remained on the hot plate for ~ 5 minutes to completely evaporate the solvents. All processes were performed inside a glove box filled with nitrogen. After casting the polymer donor layer, the samples were transferred to a vacuum chamber for deposition of the MoO₃ hole extraction layer and metal electrode. A conventional BHJ cell with a blade-coated active layer and the following device structure: ITO/Ca/PBDTTT-C-T:C₇₀ (1:1.5, 15 mg/cc)/MoO₃/Ag, was fabricated using *o*-DCB as the solvent. After fabrication, the devices were encapsulated with a UV-cured sealant (Everwide Chemical Co. Epowide EX) and cover glass under anhydrous nitrogen and measured in air. The average size of the active cell area was 5 mm². The deviation values were obtained from device-to-device variations of 4 – 8 devices. The thin films for TEM bright-field top-view investigation were prepared by immersing the glass/PEDOT:PSS/C₇₀/PBDTTT-C-T samples into deionized water. After dissolution of PEDOT:PSS, the C₇₀/PBDTTT-C-T films floated onto the water surface and were transferred to a TEM grid.⁵³ Optical constants (*n*, refractive index and *k*, extinction coefficient) of PBDTTT-C-T, C₇₀ and MoO₃ (Fig. S2) were obtained by spectroscopic ellipsometry with following procedure: the thickness of thin film was first determined by assuming *n* in the transparent region ($k=0$ at 850 – 1100 nm) to obey the Cauchy equation in fitting the ellipsometric values in the corresponding region. With the determined thickness, *n* and *k* were then varied independently across the whole spectral range of interest to fit the ellipsometric values at each wavelength (point-by-point fitting).⁵⁴

2.2 Characteristics measurements

Current density-voltage characteristics were measured with a Source Meter Keithley 2400 under AM1.5G solar illumination from a xenon lamp solar simulator (Abet Technologies) operating at 100 mW/cm² (calibrated with a NREL-traceable DG5 filtered silicon reference cell). The series resistance (R_S) and shunt resistance (R_{SH}) are estimated from the inverse slopes of the *J-V* curves at the open-circuit and short-circuit points, respectively. The external quantum efficiency spectra were obtained by illuminating periodically modulated monochromatic light with a continuous-wave bias white light (from halogen lamp) on the solar cells. The photocurrent signals were extracted with a lock-in technique that used a current preamplifier (Stanford Research

Systems) followed by a lock-in amplifier (AMETEK). The EQE measurement was entirely computer controlled, and the monochromatic light intensity was calibrated with an NIST-traceable optical power meter (OphirOptronics) (chopper frequency ~ 85 Hz). Absorption spectra were acquired with a U-3900 Spectrophotometer (Hitachi). Optical constants (refractive index, *n*, and extinction coefficient, *k*) and film thicknesses were measured using a J. A. Woollam Inc. V-VASE variable-angle spectroscopic ellipsometer. Atomic force microscopy (AFM) images were analyzed with a Bruker Dimension Icon® Atomic Force Microscope operating in tapping mode. Scanning electron microscopy (SEM) images were taken with a HitachiSU8010 microscope. A home-built panchromatic optical field simulation program, coded in Matlab™ and based on the transfer matrix method, was utilized to model optical field distributions and exciton formation.⁵⁵⁻⁵⁷ Transmission electron microscopy images were analyzed with a JEOL JEM-1200x transmission electron microscope (accelerating voltage: 120 keV). The photoluminescence emission was detected in a front-face configuration using a fiberbased spectrograph and a He-Cd laser ($\lambda = 325$ nm) as pumping source.

3. Results and discussions

3.1 Devices with toluene as solvent and optical simulation

Fig.1 shows the molecular structures of the active materials used in this study. A schematic diagram of an inverted solar cell structure with either ITO/Ca (1 nm)/C₇₀ (50 nm)/PBDTTT-C-T or PTB7/MoO₃ (7 nm)/Ag (110 nm) is also shown in Figure 1. To verify the concept, PBDTTT-C-T was first used as the donor. The PBDTTT-C-T layer was deposited onto a vacuum-sublimed C₇₀ bottom layer by blade-coating with a blade speed ranging from 60 to 350 mm/s. The blade speed dependent PBDTTT-C-T thickness is shown in Fig.S1. Utilizing toluene as the solvent for PBDTTT-C-T enabled the fabrication of a “bilayer” device with a small intermixing zone because C₇₀ has a low solubility in toluene (1.4 mg/ml). Fig.2(a) shows the short circuit current (*J*_{sc}) and power conversion efficiency (PCE) of toluene-cast devices. The simulated PCE values were obtained from a home-made optical field calculation program with assumption of 10-nm exciton diffusion length in both polymer and fullerene and experimental acquired V_{oc} ~ 0.72 and FF ~ 0.65 .⁵⁸ The optimal device had a PBDTTT-C-T thickness of ~ 40 nm.

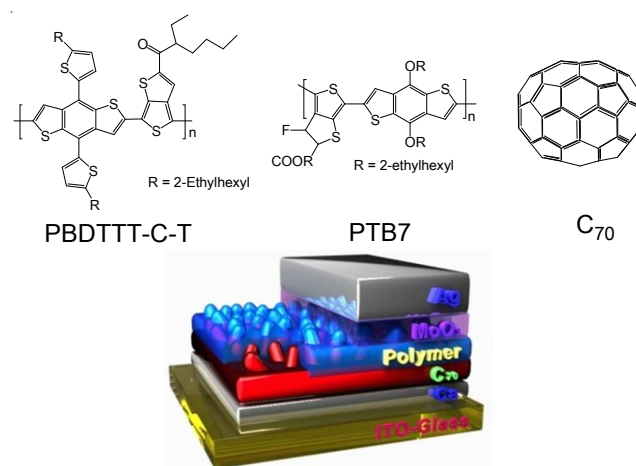


Figure 1. Device schematic and chemical structures of PBDTTT-C-T, PTB7 and C₇₀.

Devices with thicker or thinner PBDTTT-C-T layers demonstrated inferior performance. It is hypothesized that the short exciton diffusion length (L_{ex}) of organic semiconductors (~ 10 nm) plays a critical role in these results.⁵⁸ Placing the donor/acceptor interface of the bilayer device at the resonant peak of the optical field was necessary to optimize the light harvesting efficiency. **Fig. 2(b)** shows the calculated optical field distribution of devices with various PBDTTT-C-T thicknesses. It indicates that a PBDTTT-C-T thickness of ~ 40 nm and a MoO₃ optical spacer of 7 nm enhanced the optical field strength near the donor/acceptor interface, which explains the high value for J_{sc} that was observed for the 40 nm PBDTTT-C-T cell. Additionally, a maximum J_{sc} value of 11.0 mA/cm² and PCE of up to 5.08% were obtained (device characteristics are summarized in **Fig.S3, S4** and **Table S2**).

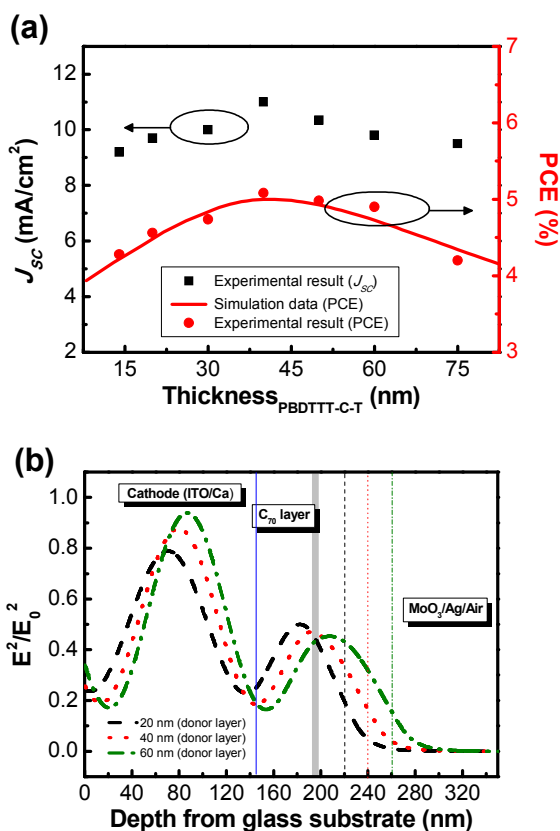


Figure 2. (a) Measured J_{sc} (black squares), PCE (red circle) and simulated PCE (red line) of C₇₀/PBDTTT-C-T devices with varying PBDTTT-C-T layer thickness and (b) optical field distributions of devices with varying PBDTTT-C-T layer thickness at the maximum absorption wavelength of 500 nm. The gray line represents the donor/acceptor interface. Device structure: ITO/Ca (1 nm)/C₇₀ (50 nm)/PBDTTT-C-T/MoO₃ (7 nm)/Ag (110 nm).

3.2 Fabrication and morphological characteristics of co-solvent (toluene:*o*-xylene) cells and conventional BHJ devices

Manipulating the degree of intermixing near the donor/acceptor interface had the following 2 advantages: (1) improved exciton dissociation efficiency by increasing the surface area of the donor/acceptor junction and (2) the *in-situ* formation of a favorable vertical phase separation for smooth carrier transport. Compared to toluene, C₇₀ is slightly more soluble in the non-halogenated solvent *o*-xylene. By controlling the co-solvent ratio (toluene:*o*-xylene) of the upper polymer

solution, the intermixing of the polymer and bottom C₇₀ layer was continuously tuned. Both the “quasi-bilayer” devices, fabricated with varying proportions of *o*-xylene that ranged from 0 to 20 wt%, and conventional BHJ reference cells were characterized. The device parameters, R_s and R_{SH} are summarized in **Fig. 3** and **Table 1**. The optimal cell, which was produced with (toluene:*o*-xylene = 95:5, wt%), had the highest PCE of 5.84%, an open circuit voltage (V_{oc}) = 0.70 V, J_{sc} = 12.3 mA/cm², and FF = 0.68. Compared to the cell fabricated using pure toluene (PCE = 5.08%, V_{oc} = 0.72 V, J_{sc} = 11.0 mA/cm², and FF = 0.64), adding *o*-xylene during production mainly increased the device J_{sc} . This is attributed to the increased donor/acceptor interface that occurred by intermixing the donor and acceptor layers. Interestingly, the cells (toluene:*o*-xylene = 100:0–90:10, wt%) all exhibited a similar R_s and R_{SH} , which may indicate a good phase separation and the reduction of charge recombination in the intermixing region.⁵⁹ Moreover, a comparable or slightly higher FF was observed in cells that were processed with 1–10 wt% co-solvent. This indicates that a certain vertical phase separation was maintained, as was observed in the bilayer case, and that the carriers were able to travel easily to the electrodes. However, with the addition of too much *o*-xylene (20 wt%), the advantageous vertical phase separation began to dissipate, and the devices had lower J_{sc} , FF and PCE values. The extreme case of complete mixing of C₇₀ and PBDTTT-C-T was represented by a BHJ reference cell. Unlike the quasi-bilayer devices, the BHJ device fabricated using *o*-DCB as solvent showed poor performance, which can be attributed to undesirable bulk and vertical phase separation.

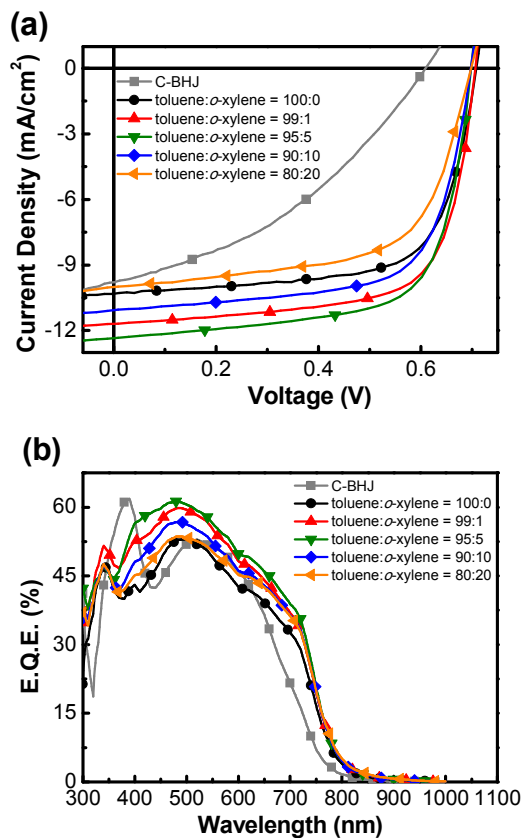


Figure 3. (a) J - V characteristics under 1 sun simulated AM1.5G illumination, and (b) the EQE spectra of the conventional bulk heterojunction (C-BHJ) device and quasi-bilayer devices fabricated using various co-solvent ratios (toluene:*o*-xylene, wt%). Quasi-bilayer device structure: ITO/Ca (1 nm)/C₇₀ (50 nm)/PBDTTT-C-T (40 nm)/MoO₃ (7 nm)/Ag (110 nm).

From the EQE results shown in Fig. 3(b), the optimal (toluene:*o*-xylene = 95:5, wt%) device showed enhanced light harvesting efficiency over the wavelength range from 350 nm to 850 nm, compared to the (toluene:*o*-xylene = 100:0, wt%) device. To clarify whether the apparent higher current density and EQE of the (toluene:*o*-xylene = 95:5, wt%) device was caused by increased photon absorption or a higher exciton dissociation efficiency, UV-Vis spectroscopy was performed on the C₇₀ neat film, the PBDTTT-C-T neat film, and the C₇₀/PBDTTT-C-T thin films coated on fused silica substrates. The preparation conditions were kept the same as for the device fabrication.

As indicated in Fig. 4, the absorption spectra of the C₇₀/PBDTTT-C-T thin films displayed the approximate combinatorial absorption of the C₇₀ and PBDTTT-C-T neat films. This demonstrates that the donor was successfully deposited on top of the C₇₀ layer by the rapid-drying blade-coating technique. In addition, the (toluene:*o*-xylene = 95:5, wt%) and (toluene:*o*-xylene = 80:20, wt%) films had a lower absorbance than the (toluene:*o*-xylene = 100:0, wt%) device, which was observed at 450 – 600 nm. This can be attributed to the slight decrease in thickness of the C₇₀ layer, which was possibly eliminated by the *o*-xylene solvent. The UV-Vis absorption results clearly indicate that the amount of photon absorption in the (toluene:*o*-xylene = 95:5, wt%) cell was almost identical or even slightly lower than in the (toluene:*o*-xylene = 100:0, wt%) device.

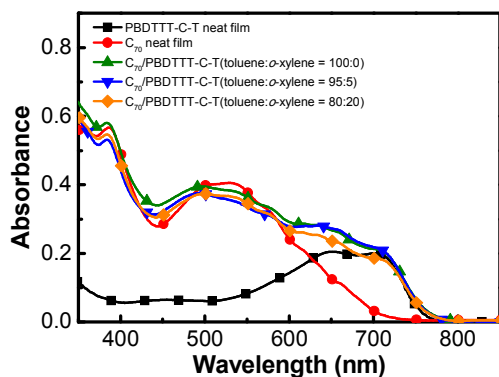


Figure 4. Absorption spectra of the 40-nm PBDTTT-C-T neat film, 50-nm C₇₀ neat film, and C₇₀ (50 nm)/PBDTTT-C-T (40 nm), the PBDTTT-C-T layers were prepared by (toluene:*o*-xylene = 100:0, wt%), (toluene:*o*-xylene = 95:5, wt%) and (toluene:*o*-xylene = 80:20, wt%) solutions.

Thus, the higher J_{sc} and EQE of the (toluene:*o*-xylene = 95:5, wt%) device can only be attributed to a higher exciton dissociation efficiency, which is because of a larger donor/acceptor interface. Furthermore, by comparison of the PBDTTT-C-T neat film and C₇₀/PBDTTT-C-T thin-film photoluminescence (PL) emission at 820 nm (the emission of

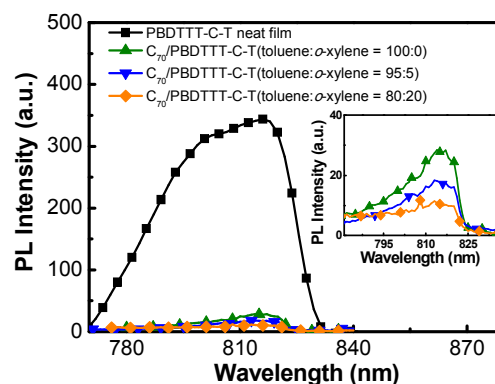


Figure 5. The front-face PL of PBDTTT-C-T (40 nm) neat film and C₇₀ (50 nm)/PBDTTT-C-T (40 nm) thin films, the PBDTTT-C-T layers were prepared by (toluene:*o*-xylene = 100:0, wt%), (toluene:*o*-xylene = 95:5, wt%) and (toluene:*o*-xylene = 80:20, wt%) solutions. The PL data are normalized to the amount of PBDTTT-C-T thin-film absorption.

PBDTTT-C-T),⁶⁰ one observed a greater PL quenching in C₇₀/PBDTTT-C-T films prepared using higher *o*-xylene ratios (91.9% (toluene:*o*-xylene = 100:0, wt%) vs. 97.1% (toluene:*o*-xylene = 80:20, wt%)), indicating more efficient charge transfer and intermixing between PBDTTT-C-T and C₇₀ (Fig. 5).⁶¹

To gain more insight on the correlation between device performance and nano-morphology of the PBDTTT-C-T/C₇₀ mixture, atomic force microscopy (AFM), transmission electron microscopy (TEM) and cross-sectional TEM measurements were performed. Whereas AFM topography only probes the surface features of the film, the structure of the intermixing layer was later examined in TEM results, which provided more detailed information on the interior of the quasi-bilayer thin films. Fig. 6 shows the surface morphology of the neat C₇₀ film and C₇₀/PBDTTT-C-T thin films, respectively. The C₇₀ neat film, which was deposited by vacuum evaporation, displayed an extremely smooth surface with a root-mean-square roughness (R_{rms}) of 0.89 nm, as shown in Fig. 6(a). After blade coating the donor on top of the C₇₀ layer with a pure toluene solution, the film (Fig. 6(b)) presented hill-like structures with a high R_{rms} of 5.95 nm. Moreover, the surface morphology of the (toluene:*o*-xylene = 95:5, wt%) and (toluene:*o*-xylene = 80:20, wt%) thin films showed even greater surface roughness with R_{rms} values of 16.2 nm and 20.1 nm, respectively (AFM characteristics are listed in Table S3). The AFM image and roughness parameter of pure polymer thin-film are shown in Fig. S7(b) and Table S3, respectively. The film showed a smooth surface with R_{rms} of 0.81 nm. The results suggest that the hill-like structures were originated from partially dissolved C₇₀ under-layers.

Table 1. Performance parameters of devices fabricated by various co-solvent ratios.

Toluene: <i>o</i> -xylene (wt%)	V_{oc} (V)	J_{sc} (mA/cm ²)	FF	PCE [highest] (%)	R_s (Ω *cm ²)	R_{sh} (Ω *cm ²)
BHJ	0.60 ± 0.01	9.60 ± 0.18	0.37 ± 0.01	2.13 ± 0.12 [2.25]	33.5	315.3
100:0	0.70 ± 0.01	10.60 ± 0.30	0.64 ± 0.01	4.74 ± 0.29 [5.03]	12.5	807.4
99:1	0.69 ± 0.01	11.51 ± 0.19	0.68 ± 0.01	5.40 ± 0.28 [5.68]	8.9	977.6
95:5	0.69 ± 0.01	12.12 ± 0.18	0.68 ± 0.01	5.77 ± 0.07 [5.84]	8.41	993.1
90:10	0.68 ± 0.01	10.81 ± 0.19	0.66 ± 0.01	4.85 ± 0.32 [5.17]	10.5	980.3
80:20	0.68 ± 0.01	9.51 ± 0.49	0.61 ± 0.01	3.94 ± 0.35 [4.29]	13.2	540.9

Cite this: DOI: 10.1039/c0xx00000x

www.rsc.org/xxxxxx

Full Article

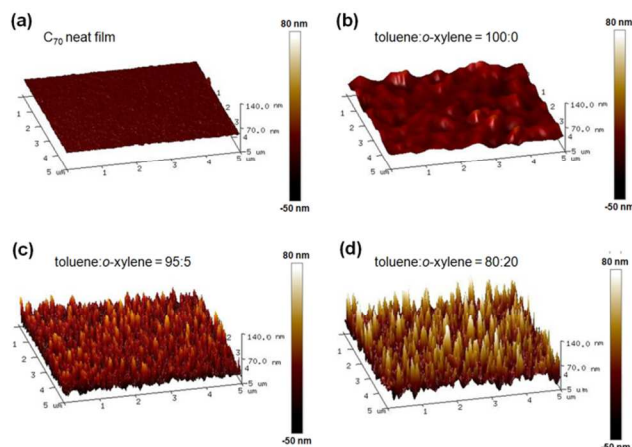


Figure 6. AFM images of the (a) C_{70} (50 nm) neat film, (b) C_{70} (50 nm)/PBDTTT-C-T (40 nm) (toluene:*o*-xylene = 100:0, wt%) thin film, (c) C_{70} (50 nm)/PBDTTT-C-T (40 nm) (toluene:*o*-xylene = 95:5, wt%) thin film, and (d) C_{70} (50 nm)/PBDTTT-C-T (40 nm) (toluene:*o*-xylene = 80:20, wt%) thin film.

The changes in nano-morphology of the C_{70} /PBDTTT-C-T quasi-bilayer using various proportions of *o*-xylene co-solvent were more apparent in bright-field TEM images, as shown in **Fig. 7** (focused) and **Fig. S5** (defocused). Notably, the TEM images reveal randomly oriented, island-like nano-structures. The density and contrast of these island-like nano-structures increased with *o*-xylene wt%, which is consistent with the AFM result. The variation in image contrast could result from different composition or thin-film thickness. The electron density of fullerenes has been observed to be higher than that of polymers.^{28, 40, 62-65} As a result, the higher mass-thickness contrast of C_{70} gives the dark C_{70} -rich domains from the bright region of PBDTTT-C-T-rich matrix. TEM images show the island-like nano-structures which is consistent with the SEM image (inset of **Fig. 7(b)**). In contrast, the SEM image of (toluene:*o*-xylene = 95:5, wt%) PBDTTT-C-T neat film showed a smooth surface (**Fig. S7(a)**). Accordingly, the island-like nano-structures could represent a certain degree of C_{70} aggregation, which is likely attributed to the selective solubility of C_{70} and PBDTTT-C-T in toluene and *o*-xylene. The (toluene:*o*-xylene = 95:5, wt%) and (toluene:*o*-xylene = 80:20, wt%) films showed a higher density of island-like nano-structures compared to the (toluene:*o*-xylene = 100:0, wt%) one, which could be beneficial to the larger donor/acceptor interface.

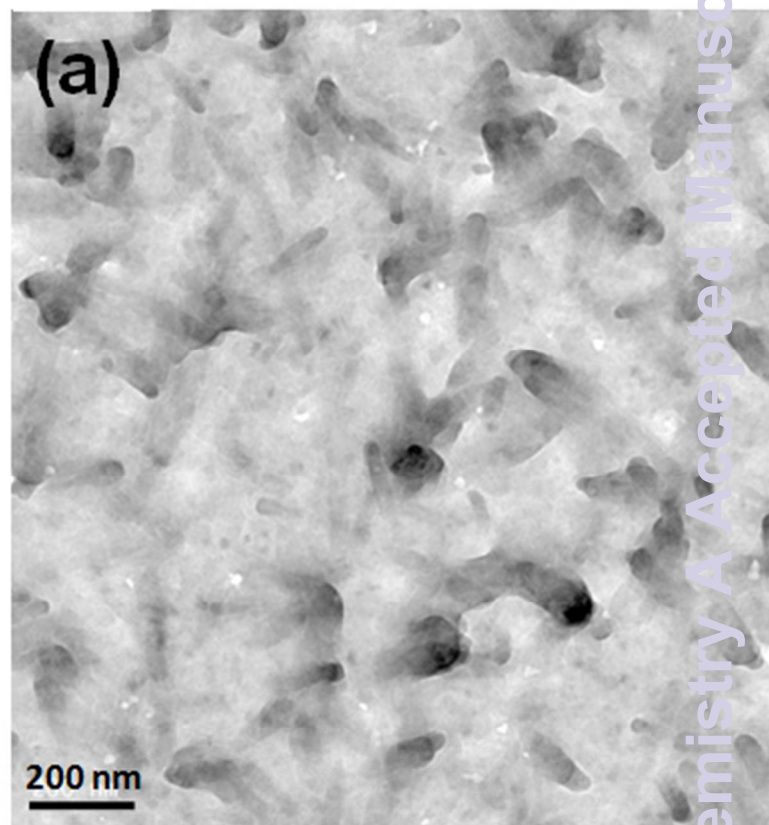


Figure 7. TEM micrographs of C_{70} (50 nm)/PBDTTT-C-T (40 nm) thin films, the PBDTTT-C-T layers were prepared by (a) (toluene:*o*-xylene = 100:0, wt%), (b) (toluene:*o*-xylene = 95:5, wt%), and (c) (toluene:*o*-xylene = 80:20, wt%) solutions. The inset of (b) shows 45 degree of SEM image with same condition as (b).

To acquire more information on the nano-morphology of the device, cross-sectional TEM images prepared by two different slicing methods were investigated (detail processes shown in **Fig. S7**). **Fig. 8** and **Fig. S7(a)** show the cross-sectional TEM images with the following structure: ITO/PEDOT:PSS (40 nm)/ C_{70} (60 nm)/PBDTTT-C-T (toluene:*o*-xylene = 95:5, wt%)/Al at different magnification. The wavy interface of the donor and acceptor layers can be resolved, indicating that the donor and acceptor layers were not well-mixed in the process. The images also display a vertical contrast in the active layer. The brighter upper region is distinguished from the darker lower region, implying that the active layer gradually changes from C_{70} -rich to PBDTTT-C-T-rich matrix from the bottom to the top and the formation of diffusive quasi-bilayer structure. Referring to the AFM, TEM and SEM results, an illustration of the quasi-bilayer with island-like nano-structures is shown in **Fig. 9**. By selecting non-halogenated solvents with two different C_{70} solubilities and using the rapid-drying blade-coating method, we fabricated a controllable inter-diffusive quasi-bilayer that increased device performance. The increased surface roughness and large mixture layer observed in the (toluene:*o*-xylene = 80:20, wt%) thin film may have caused direct contact of PBDTTT-C-T with the cathode

and/or C_{70} with the anode which could lead to leakage current and lower device performance.

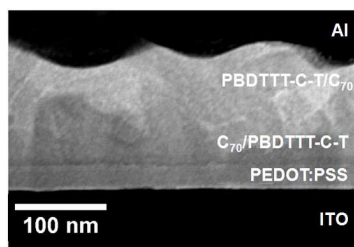


Figure 8. Cross-sectional TEM image (30000x) of ITO/PEDOT:PSS (40 nm)/ C_{70} (60 nm)/PBDTTT-C-T (toluene:*o*-xylene = 95:5, wt%) (40 nm)/Al.

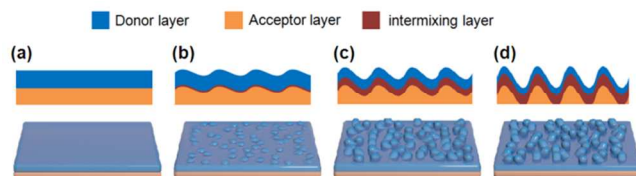


Figure 9. Illustration of the thin-film morphologies of (a) conventional bilayer, (b) C_{70} /PBDTTT-C-T film (toluene:*o*-xylene = 100:0, wt%), (c) C_{70} /PBDTTT-C-T film (toluene:*o*-xylene = 95:5, wt%) and (d) C_{70} /PBDTTT-C-T film (toluene:*o*-xylene = 80:20, wt%).

3.3 Devices with optimized C_{70} and MoO_3 thickness

Because there was a thicker intermixing layer in devices fabricated with a (toluene:*o*-xylene = 95:5, wt%) co-solvent, the optimal thickness of C_{70} for these devices may not be the same thickness that was determined for toluene-fabricated cells. Therefore, the thickness of C_{70} was first optimized for the purpose of maximizing the optical field distribution in the active layer. The device parameters are summarized in **Table 2** and the *J-V* characteristics are shown in **Fig. 10-11**. As shown in the inset of **Fig. 10**, the optimal device (60 nm C_{70}) showed an

Table 2. Performance parameters of devices with various C_{70} and MoO_3 layer thicknesses.

Thickness of C_{70}	Thickness of MoO_3	V_{oc} (V)	J_{sc} (mA/cm ²)	FF	PCE [highest] (%)
30 nm	7 nm	0.69 ± 0.01	11.80 ± 0.12	0.64 ± 0.02	5.12 ± 0.11 [5.23]
40 nm	7 nm	0.69 ± 0.01	11.65 ± 0.15	0.68 ± 0.01	5.46 ± 0.30 [5.76]
50 nm	7 nm	0.69 ± 0.01	12.20 ± 0.10	0.67 ± 0.01	5.64 ± 0.20 [5.84]
60 nm	7 nm	0.70 ± 0.02	13.17 ± 0.13	0.66 ± 0.01	6.08 ± 0.38 [6.46]
70 nm	7 nm	0.68 ± 0.01	12.50 ± 0.20	0.61 ± 0.01	5.61 ± 0.29 [5.90]
60 nm	3 nm	0.68 ± 0.01	12.42 ± 0.38	0.59 ± 0.02	4.98 ± 0.51 [5.49]
60 nm	7 nm	0.71 ± 0.01	13.13 ± 0.15	0.66 ± 0.01	6.15 ± 0.31 [6.46]
60 nm	10 nm	0.70 ± 0.01	13.50 ± 0.10	0.66 ± 0.01	6.23 ± 0.32 [6.55]
60 nm	15 nm	0.70 ± 0.01	13.03 ± 0.17	0.67 ± 0.01	6.11 ± 0.09 [6.20]
60 nm	20 nm	0.68 ± 0.01	12.22 ± 0.28	0.64 ± 0.01	5.32 ± 0.59 [5.91]

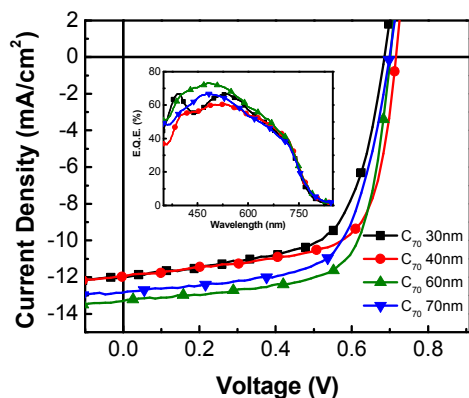


Figure 10. *J-V* characteristics of devices with various C_{70} layer thicknesses. The inset shows the corresponding EQE spectra. Device structure: ITO/Ca (1 nm)/ C_{70} /PBDTTT-C-T (40 nm)/ MoO_3 (7 nm)/Ag (110 nm).

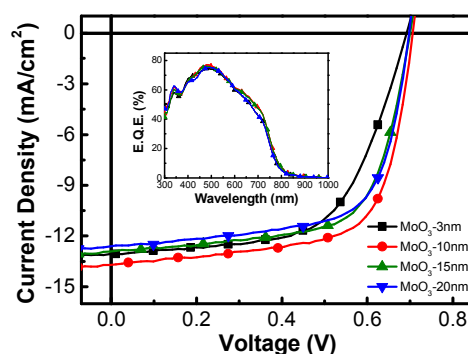


Figure 11. *J-V* characteristics of devices with various MoO_3 layer thickness. The inset shows the corresponding EQE spectra. Device structure: ITO/Ca (1 nm)/ C_{70} (60 nm)/PBDTTT-C-T (40 nm)/ MoO_3 /Ag (110 nm).

increased EQE value of up to ~70% within the wavelength range of 400 – 550 nm, which corresponds to C_{70} absorption. The device possessed a V_{oc} = 0.72 V, J_{sc} = 13.3 mA/cm², FF = 0.67, and delivered a PCE of up to 6.46%.

The AFM and TEM results suggest that 7 nm MoO_3 may not fully cover the active quasi-bilayer with high surface roughness. We then fine-tuned the thickness of MoO_3 to further optimize device performance. As shown in **Fig. 11**, the device with 3 nm MoO_3 performed the poorest among all the cells. This is because low coverage of the MoO_3 layer caused direct contact of the active layer with the exciton quenching metal electrode.⁶⁶

Increasing MoO₃ thickness significantly improved device performance. However, efficiency decreased in devices with >10 nm MoO₃, which can be attributed to the effect of optical resonance inside the active layer. As a result, the optimal device with a 10 nm layer of MoO₃ gave an impressive performance with V_{oc} = 0.71 V, J_{sc} = 13.6 mA/cm², FF = 0.68, and a PCE as high as 6.55%.

For comparison, ZnO and CsF were also utilized as electron extraction layers in this study. However, they all demonstrated lower PCEs in the range of 2.17% – 4.27% (see Fig. S8-S11 and Table S4, S5). This could have been caused by increased charge recombination or higher surface roughness of the ZnO and CsF layers. A detailed mechanism is still under investigation.

3.4 Devices with a PTB7 donor layer

To demonstrate that the approach proposed in this study can be widely adopted in various polymer systems, we used PTB7 as the donor layer in a quasi-bilayer device. The fabrication process and device structure were the same as for the optimized PBDTTT-C-T devices: ITO/Ca (1 nm)/C₇₀ (60nm)/PTB7 (20 – 100 nm, toluene:*o*-xylene = 95:5, wt^o)/MoO₃ (10 nm)/Ag (110 nm). The J-V characteristics and EQE spectra of these devices are shown in Fig. 12, Fig. S12-S14 and Table S6-S7. Tuning the thickness of the PTB7 layer showed a trade-off between J_{sc} and FF. The optimal thickness of PTB7 was determined to be 70 nm, which delivered a PCE of up to 7.01% ± 0.14% [max 7.15%], V_{oc} = 0.69 ± 0.01 V [max 0.70 V], J_{sc} = 13.9 ± 0.2 mA/cm² [max 14.1 mA/cm²], and FF = 72.1 ± 0.09 % [max 73.0 %]. This efficiency is comparable to PTB7BHJ solar cells fabricated using halogenated solvents and additives.⁵⁰

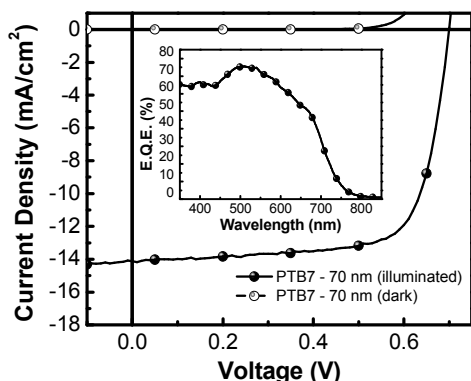


Figure 12. J-V characteristics of devices with a 70 nm PTB7 layer. The inset shows the corresponding EQE spectrum. Device structure: ITO/Ca (1 nm)/C₇₀(60 nm)/PTB7 (70 nm)/MoO₃(10 nm)/Ag (110 nm).

Intensity dependent device performance of the optimal PTB7 quasi-bilayer solar cell is shown in Fig. S13 in the supporting information. The device demonstrated higher efficiency under low illumination. The PCE reached a maximum of ~8% at a simulated light intensity of ~0.08 sun.

4. Conclusions

In summary, we have conceptually demonstrated the fabrication of inverted quasi-bilayer OSCs by utilizing poorly soluble vacuum-deposited C₇₀ and non-halogenated solvent deposited polymers. The interfacial interpenetration mixture was continuously controlled by tuning the compositional ratio of the toluene:*o*-xylene co-solvent. The correlation between device

performance and thin-film nano-morphology was comprehensively studied using AFM, TEM, SEM, cross-sectional TEM and PL quenching measurement. An unusual island-like morphology was observed. After engineering the donor/acceptor interface and optimizing device optics and morphology, PBDTTT-C-T and PTB7 cells demonstrated high PCEs of up to 6.55% and 7.15% under simulated 1-sun illumination, respectively. The PTB7 device showed a higher PCE of ~8% at low illumination intensity (0.08 sun). These efficiencies are comparable to state-of-the-art BHJ devices fabricated using halogenated solvents. The cells developed in this study have the following three advantages over traditional BHJ devices: (1) the enhanced control over the BHJ offered by quasi-bilayer processing when compared to blend casting; (2) the mixture of the bottom C₇₀ layer and the upper polymer layer occurred within 1 second without long-time solvent or thermal annealing; and (3) the halogenated-solvent-free fabrication conforms to the halogen-free compliance. Our results provide important insight into novel device structures and fabrication processes, which may trigger advanced efforts in the production of non-toxic, fast-throughput, and large-area OSCs.

Acknowledgements

The authors would like to acknowledge the financial support from the National Science Council of Taiwan (NSC-102-2221-E-007-125-MY3, NSC-101-2112-M-007-017-MY3) and the Low Carbon Energy Research Center, National Tsing Hua University.

Notes and references

^aDepartment of Materials Science and Engineering, National Tsing Hua University, No. 101, Section 2, Kuang-Fu Road, Hsinchu, Taiwan 30013. E-mail: hwlin@mx.nthu.edu.tw

^bDepartment of Chemical Engineering, National Tsing Hua University, No. 101, Section 2, Kuang-Fu Road, Hsinchu, Taiwan 30013.

^cInstitute of Physics, National Chiao Tung University, Hsinchu, Taiwan 30013.

† Electronic Supplementary Information (ESI) available. See DOI: 10.1039/b000000x/

1. C. W. Tang, *Appl. Phys. Lett.*, 1986, **48**, 183.
2. L. Huo, J. Hou, S. Zhang, H.-Y. Chen and Y. Yang, *Angew. Chem.*, 2010, **122**, 1542-1545.
3. S. Sista, M. H. Park, Z. Hong, Y. Wu, J. Hou, W. L. Kwan, G. Li and Y. Yang, *Adv. Mater.*, 2010, **22**, 380-383.
4. V. Steinmann, N. M. Kronenberg, M. R. Lenze, S. M. Graf, D. Hertel, K. Meerholz, H. Bürckstümmer, E. V. Tulyakova and F. Würthner, *Adv. Energy Mater.*, 2011, **1**, 888-893.
5. Y. H. Chen, L. Y. Lin, C. W. Lu, F. Lin, Z. Y. Huang, H. W. Lin, P. H. Wang, Y. H. Liu, K. T. Wong, J. Wen, D. J. Miller and S. B. Darling, *J. Am. Chem. Soc.*, 2012, **134**, 13616-13623.
6. R. Grisorio, G. Allegretta, G. P. Suranna, P. Mastrorilli, A. Loiudice, A. Rizzo, M. Mazzeo and G. Gigli, *J. Mater. Chem.*, 2012, **22**, 19752.
7. H.-W. Lin, Y.-H. Chen, Z.-Y. Huang, C.-W. Chen, L.-Y. Lin, F. Lin and K.-T. Wong, *Org. Electron.*, 2012, **13**, 1722-1728.
8. L. Zhang, B. Walker, F. Liu, N. S. Colella, S. C. B. Mannsfeld, J. J. Watkins, T.-Q. Nguyen and A. L. Briseno, *J. Mater. Chem.*, 2012, **22**, 4266.

9. S. H. Park, A. Roy, S. Beaupré, S. Cho, N. Coates, J. S. Moon, D. Moses, M. Leclerc, K. Lee and A. J. Heeger, *Nature Photon.*, 2009, **3**, 297-302.
10. C. Piliago, T. W. Holcombe, J. D. Douglas, C. H. Woo, P. M. Beaujuge and J. M. Frechet, *J. Am. Chem. Soc.*, 2010, **132**, 7595-7597.
11. T. Y. Chu, J. Lu, S. Beaupre, Y. Zhang, J. R. Pouliot, S. Wakim, J. Zhou, M. Leclerc, Z. Li, J. Ding and Y. Tao, *J. Am. Chem. Soc.*, 2011, **133**, 4250-4253.
12. H. Zhou, L. Yang, S. C. Price, K. J. Knight and W. You, *Angew. Chem. Int. Ed.*, 2010, **49**, 7992-7995.
13. Y. Liang and L. Yu, *Acc. Chem. Res.*, 2010, **43**, 1227-1236.
14. V. Gupta, A. K. Kyaw, D. H. Wang, S. Chand, G. C. Bazan and A. J. Heeger, *Scientific reports*, 2013, **3**, 1965.
15. S. B. Darling and F. You, *RSC Advances*, 2013, **3**, 17633.
16. C.-C. Chen, L. Dou, J. Gao, W.-H. Chang, G. Li and Y. Yang, *Energy Environ. Sci.*, 2013, **6**, 2714.
17. D. Yu, Y. Yang, M. Durstock, J. B. Baek and L. Dai, *ACS Nano*, 2010, **4**, 5633-5640.
18. H. Kageyama, H. Ohishi, M. Tanaka, Y. Ohmori and Y. Shirota, *Adv. Funct. Mater.*, 2009, **19**, 3948-3955.
19. S.-W. Liu, W.-C. Su, C.-C. Lee, C.-F. Lin, S.-C. Yeh, C.-T. Chen and J.-H. Lee, *Org. Electron.*, 2012, **13**, 2118-2129.
20. D. Yokoyama, Z. Qiang Wang, Y.-J. Pu, K. Kobayashi, J. Kido and Z. Hong, *Sol. Energy Mater. Sol. Cells*, 2012, **98**, 472-475.
21. W. Zhao, J. P. Mudrick, Y. Zheng, W. T. Hammond, Y. Yang and J. Xue, *Org. Electron.*, 2012, **13**, 129-135.
22. H.-L. Yip and A. K. Y. Jen, *Energy Environ. Sci.*, 2012, **5**, 5994.
23. T. Yang, M. Wang, C. Duan, X. Hu, L. Huang, J. Peng, F. Huang and X. Gong, *Energy Environ. Sci.*, 2012, **5**, 8208.
24. T. S. van der Poll, J. A. Love, T. Q. Nguyen and G. C. Bazan, *Adv. Mater.*, 2012, **24**, 3646-3649.
25. T. Zhang, E. Birgersson, K. Ananthanarayanan, C. H. Yong, L. N. S. A. Thummalakunta and J. Luther, *J. Appl. Phys.*, 2012, **112**, 084511.
26. A. Loidice, A. Rizzo, M. Biasiucci and G. Gigli, *The J. of Physical Chemistry Lett.*, 2012, **3**, 1908-1915.
27. D. H. Wang, J. S. Moon, J. Seifter, J. Jo, J. H. Park, O. O. Park and A. J. Heeger, *Nano Lett.*, 2011, **11**, 3163-3168.
28. J. S. Moon, C. J. Takacs, Y. Sun and A. J. Heeger, *Nano Lett.*, 2011, **11**, 1036-1039.
29. K. H. Lee, P. E. Schwenn, A. R. Smith, H. Cavaye, P. E. Shaw, M. James, K. B. Krueger, I. R. Gentle, P. Meredith and P. L. Burn, *Adv. Mater.*, 2011, **23**, 766-770.
30. V. S. Gevaerts, L. J. Koster, M. M. Wienk and R. A. Janssen, *ACS applied materials & interfaces*, 2011, **3**, 3252-3255.
31. D. Chen, F. Liu, C. Wang, A. Nakahara and T. P. Russell, *Nano Lett.*, 2011, **11**, 2071-2078.
32. A. L. Ayzner, C. J. Tassone, S. H. Tolbert and B. J. Schwartz, *J. Phys. Chem. C*, 2009, **113**, 20050-20060.
33. G. Li, V. Shrotriya, J. Huang, Y. Yao, T. Moriarty, K. Emery and Y. Yang, *Nat. Mater.*, 2005, **4**, 864-868.
34. H.-Y. Chen, J. Hou, S. Zhang, Y. Liang, G. Yang, Y. Yang, L. Yu, Y. Wu and G. Li, *Nature Photon.*, 2009, **3**, 649-653.
35. S. Kwon, J. K. Park, G. Kim, J. Kong, G. C. Bazan and K. Lee, *Adv. Energy Mater.*, 2012, **2**, 1420-1424.
36. Y. Sun, G. C. Welch, W. L. Leong, C. J. Takacs, G. C. Bazan and A. J. Heeger, *Nat. Mater.*, 2012, **11**, 44-48.
37. K. Tada and M. Onoda, *Jpn. J. Appl. Phys.*, 2012, **51**, 030205.
38. C.-D. Park, T. A. Fleetham, J. Li and B. D. Vogt, *Org. Electron.*, 2011, **12**, 1465-1470.
39. D. Yue, P. Khatav, F. You and S. B. Darling, *Energy Environ. Sci.*, 2012, **5**, 9163.
40. K.-S. Chen, H.-L. Yip, C. W. Schlenker, D. S. Ginger and A. K. Y. Jen, *Org. Electron.*, 2012, **13**, 2870-2878.
41. H.-C. Liao, C.-C. Ho, C.-Y. Chang, M.-H. Jao, S. B. Darling and W.-F. Su, *Mater. Today*, 2013, **16**, 326-336.
42. Y.-C. Chao, S.-Y. Huang, C.-Y. Chen, Y.-F. Chang, H.-F. Meng, F.-W. Yen, I. F. Lin, H.-W. Zan and S.-F. Horng, *Synth. Met.*, 2011, **161**, 148-152.
43. J.-H. Chang, Y.-H. Chen, H.-W. Lin, Y.-T. Lin, H.-F. Meng and E.-C. Chen, *Org. Electron.*, 2012, **13**, 705-709.
44. W. Chen, M. P. Nikiforov and S. B. Darling, *Energy Environ. Sci.*, 2012, **5**, 8045.
45. S. Rajaram, R. Shivanna, S. K. Kandappa and K. S. Narayan, *The J. of Physical Chemistry Lett.*, 2012, **3**, 2405-2408.
46. X. Li, W. C. Choy, L. Huo, F. Xie, W. E. Sha, B. Ding, X. Guo, Y. Li, J. Hou, J. You and Y. Yang, *Adv. Mater.*, 2012, **24**, 3046-3052.
47. K.-S. Chen, J.-F. Salinas, H.-L. Yip, L. Huo, J. Hou and A. K. Y. Jen, *Energy Environ. Sci.*, 2012, **5**, 9551.
48. Z. He, C. Zhong, S. Su, M. Xu, H. Wu and Y. Cao, *Nature Photon.*, 2012, **6**, 593-597.
49. W. Chen, T. Xu, F. He, W. Wang, C. Wang, J. Strzalka, Y. Liu, J. Wen, D. J. Miller, J. Chen, K. Hong, L. Yu and S. B. Darling, *Nano Lett.*, 2011, **11**, 3707-3713.
50. H. Zhou, Y. Zhang, J. Seifter, S. D. Collins, C. Luo, G. C. Bazan, T. Q. Nguyen and A. J. Heeger, *Adv. Mater.*, 2013, **25**, 1646-1652.
51. Y. Liang, Z. Xu, J. Xia, S. T. Tsai, Y. Wu, G. Li, C. Ray and L. Yu, *Adv. Mater.*, 2010, **22**, E135-138.
52. B. A. Collins, Z. Li, J. R. Tumbleston, E. Gann, C. R. McNeill and H. Ade, *Adv. Energy Mater.*, 2013, **3**, 65-74.
53. M. Reyes-Reyes, R. Lopez-Sandoval, J. Arenas-Alatorre, R. Garibay-Alonso, D. L. Carroll and A. Lastras-Martinez, *Thin Solid Films*, 2007, **516**, 52-57.
54. H. W. Lin, C. L. Lin, H. H. Chang, Y. T. Lin, C. C. Wu, Y. M. Chen, R. T. Chen, Y. Y. Chien and K. T. Wong, *J. Appl. Phys.*, 2004, **95**, 881-886.
55. H. W. Lin, S. W. Chiu, L. Y. Lin, Z. Y. Hung, Y. H. Chen, F. Lin and K. T. Wong, *Adv. Mater.*, 2012, **24**, 2269-2272.
56. R. Fitzner, E. Reinold, A. Mishra, E. Mena-Osteritz, H. Ziehlke, C. Körner, K. Leo, M. Riede, M. Weil, O. Tsaryova, A. Weiß, C. Uhrich, M. Pfeiffer and P. Bäuerle, *Adv. Funct. Mater.*, 2011, **21**, 897-910.
57. L. A. A. Pettersson, L. S. Roman and O. Inganäs, *J. Appl. Phys.*, 1999, **86**, 487.
58. L. Y. Lin, Y. H. Chen, Z. Y. Huang, H. W. Lin, S. H. Chou, F. Lin, C. W. Chen, Y. H. Liu and K. T. Wong, *J. Am. Chem. Soc.*, 2011, **133**, 15822-15825.
59. M. S. Kim, B. G. Kim and J. Kim, *ACS applied materials & interfaces*, 2009, **1**, 1264-1269.
60. R. Shivanna, S. Shoaee, S. Dimitrov, S. K. Kandappa, S. Rajaram, J. Durrant and K. S. Narayan, *Energy Environ. Sci.*, 2013.

-
61. V. Vohra, K. Higashimine, T. Murakami and H. Murata, *Appl. Phys. Lett.*, 2012, **101**, 173301.
62. X. Yu, K. Yue, I. F. Hsieh, Y. Li, X. H. Dong, C. Liu, Y. Xin, H. F. Wang, A. C. Shi, G. R. Newkome, R. M. Ho, E. Q. Chen, W. B. Zhang and S. Z. Cheng, *Proceedings of the National Academy of Sciences of the United States of America*, 2013, **110**, 10078-10083.
63. X. Yang, J. K. J. van Duren, R. A. J. Janssen, M. A. J. Michels and J. Loos, *Macromolecules*, 2004, **37**, 2151-2158.
64. L. Huo, L. Ye, Y. Wu, Z. Li, X. Guo, M. Zhang, S. Zhang and J. Hou, *Macromolecules*, 2012, **45**, 6923-6929.
65. C. M. Amb, S. Chen, K. R. Graham, J. Subbiah, C. E. Small, F. So and J. R. Reynolds, *J. Am. Chem. Soc.*, 2011, **133**, 10062-10065.
66. J. D. Servaites, M. A. Ratner and T. J. Marks, *Energy Environ. Sci.*, 2011, **4**, 4410.

15

Graphical Abstract

